

Exploring the spatiotemporal evolution patterns of Urban Heat Island with a network-based approach

Kang Zou ^a, Xinyu Yu ^a, Man Sing Wong ^{a,b,*}, Kai Qin ^c, Rui Zhu ^d, Songyang Li ^a

^a Department of Land Surveying and Geo-Informatics, The Hong Kong Polytechnic University, Hung Hom, Hong Kong, China

^b Research Institute for Sustainable Urban Development, The Hong Kong Polytechnic University, Hung Hom, Hong Kong, China

^c School of Environment Science and Spatial Informatics, China University of Mining and Technology, Xuzhou, China

^d Institute of High Performance Computing (IHPC), Agency for Science, Technology and Research (A*STAR), Republic of Singapore

ARTICLE INFO

Keywords:

Surface urban heat island
Urban expansion
Spatiotemporal patterns
Cellular Automata

ABSTRACT

Exploring the development patterns of surface urban heat island (SUHI) has become crucial for formulating corresponding excess heat mitigation measures. However, there is currently a lack of analysis on the importance and interactions of different SUHI patches. This paper proposes a simple and effective method for measuring SUHI patterns, revealing the development patterns and growth trends of SUHI through spatial integration and interaction network construction. The results show that the values of nodes and edges in the SUHI network have continuously increased from 2005 to 2020, with an increase of the average importance index of nodes and the average interaction intensity of edges in the three regions by 40.2% and 23.6%, respectively. Moreover, the development pattern of SUHI exhibits a distinct unimodal characteristic. When the merging speed of SUHI patches exceeds the speed of new patch emergence, the total number of patches will decrease. The method proposed in this study demonstrates strong applicability across the three urban agglomerations and can be extended to other regions. The SUHI network enables the practical and efficient excess heat mitigation of heat island effects through the management (disruption) of key nodes. The corresponding heat island development hypothesis also enriches the theoretical understanding of heat island development.

1. Introduction

The urban heat island (UHI) phenomenon has been exacerbating due to the impacts of global warming as well as city expansion. The rapid urban sprawl and changes in impervious surfaces, resulting from population growth and anthropogenic activities, have contributed significantly to this issue (Wang et al., 2018b; Zinzi et al., 2020). With large fossil fuel consumption, significant alterations in the urban surface characteristics and excessive greenhouse gases have resulted in a profound impact on the urban climate, accelerating the worsening of the UHI effect, leading to issues such as drought and water shortages, power supply shortages, and loss of biodiversity, with such incidents occurring daily in many countries (Yang et al., 2021a; Mazdiyasni and Agha-Kouchak, 2015; Cornes and Cook, 2018). Generally, the UHI effect can be categorized into two major types: atmospheric UHI (AUHI), which includes boundary-layer UHI (BUHI) and canopy-layer UHI (CUHI), and surface UHI (SUHI) (Oke et al., 2017). Currently, satellite-based land

surface temperature (LST) products have been widely used for SUHI investigation as they can compensate for the under-representation of in-situ temperature measurements over the entire space (Zhou et al., 2022). Therefore, satellite-based LST observations enable the measurement of SUHI effects from a broader spatial perspective, which is the focus of this study (Yao et al., 2017; Deilami et al., 2018).

In spatial terms, varying background climates and urban development strategies manifest in different SUHI coverage patterns (Liu et al., 2021). The spatial assessment of SUHI effects can quantify the risks associated with SUHI and reveal significant disparities between urban areas, highlighting deficiencies in specific regions or zones. The findings can assist urban planning departments in formulating targeted measures (Li et al., 2023). Moreover, in temporal aspect, SUHI mitigation measures are time-sensitive, and based on past conditions, the optimal window for intervention could easily be missed (Sun et al., 2024; Yang et al., 2019). There may be significant differences in SUHI pattern between cities at different stages of development, and from a broader

* Corresponding author at: Department of Land Surveying and Geo-Informatics, The Hong Kong Polytechnic University, 181 Chatham Road South, Hung Hom, Kowloon, Hong Kong.

E-mail address: Ls.charles@polyu.edu.hk (M.S. Wong).

perspective, the potential to mitigate the risks of SUHI effects is often overlooked.

Over the years, researchers have proposed many definitions and conducted corresponding studies to assess the SUHI effect (and its intensity) (Cao et al., 2010; Lin et al., 2018; Wang et al., 2018a). For example, a widely used definition of the SUHI effect is the temperature difference between urban areas and their surrounding rural regions (Li et al., 2020). This classification provides researchers and policymakers with a straightforward and intuitive perspective to distinguish between the spatial heterogeneity of temperatures in local urban and rural areas under the background climate. However, some researchers pointed out that urban and rural areas represent a dynamic continuum rather than a dichotomy, meaning that traditional urban-rural divisions fail to accurately reflect the actual climatic conditions of cities (Montgomery, 2008; Yu et al., 2019; Jiang et al., 2024). Additionally, the elevation gradient between urban and rural areas may also affect temperature differences, suggesting that observed temperature variations might not represent actual SUHI signals (Imhoff et al., 2010). Consequently, some researchers have proposed adopting the local climate zone approach, which calculates the SUHI by defining the temperature difference between compact high-rise building categories and low-rise vegetation categories, thus overcoming the errors associated with binary classifications (Stewart and Oke., 2012; Jiang et al., 2022). Alternatively, by establishing buffer zones and excluding pixels above a certain elevation threshold, this method identifies rural reference points, thereby mitigating the impact of elevation on SUHI intensity (SUHII) measurements (Yao et al., 2018; Liu et al., 2021). At regional scale, the Gaussian model is another method used in previous studies to quantify SUHII (Yang, Huang and Tang, 2019; Lai et al., 2021). Compared with the traditional temperature dichotomy method, the impact of the urban-rural boundary on the results is less significant (Li et al., 2022). This is because the Gaussian model approach is based on fitting a plane to surface temperature data to reflect the characteristics of SUHII. Additionally, the Gaussian model can also be used to determine the spatial extent and central location of the SUHI (Streutker, 2003; Quan et al., 2014).

However, it is important to note that most previous studies are based on the superimposition of pixels from different thematic layers (Dewan et al., 2021; Meng et al., 2018; Yue et al., 2019). This pixel mosaicking approach fails to consider the overall pattern of SUHI patches and struggles to describe the connectivity between different patches. Particularly, the LST is influenced by the thermal capacity and exchange between different surface types, and the spatial connectivity between heat sources and sinks plays a crucial role in the heat flow across surface patches (Sun et al., 2018). The potential role of connectivity in influencing regional SUHI effects has increasingly been recognized. For instance, the impact of connectivity within SUHI patch areas on the intensity of SUHI effects, the propagation and characteristics of SUHI risk networks, and the analysis of SUHI patch patterns and types through connectivity-based morphological spatial patterns (Chen et al., 2019; Liu et al., 2024; Yu et al., 2021). However, current studies on the connectivity of SUHI patches are based on raster and vector data, lacking methods that describe the evolution of SUHI patterns from a network perspective (Debbage and Shepherd., 2015; Shen, 2024; Hu et al., 2022). This makes it challenging for urban decision-makers and planners to identify and measure key nodes (patches) within SUHI area to effectively mitigate excess heat.

On the other hand, with the acceleration of urbanization, both the existing and new development of construction areas inevitably leads to a reduction in the distances between patches, or even their merging, forming urban agglomerations (Fang et al., 2017; Zhou et al., 2018; Bartesaghi-Koc et al., 2020; Zhu et al., 2022). In this process, the SUHI effect often transcends traditional administrative boundaries. Some studies have acknowledged this issue. For example, Fan et al. (2017) derived from energy balance models and thermodynamic simulations that the horizontal extent of SUHI exceeds the physical boundaries of cities. Yu et al. (2019) introduced the concept of Regional Heat Islands

(RHI) to describe the phenomenon of heat environment development across regions. More importantly, as mentioned earlier, the assessment of the extent and intensity of SUHI in urban agglomerations must address the impacts of elevation and background climate as far as possible. The delineation of SUHI influences the evaluation of interaction strength and connectivity between SUHI patches. Therefore, an urban agglomeration SUHI delineation method based on the connectivity of construction land patches is crucial for blocking (or disrupting) key nodes and links in the SUHI network (Peng et al., 2022).

Consequently, this study defines a method for delineating SUHI regions and calculating their intensity based on the construction land of urban agglomerations and the overall background climate, serving to identify key patches and assess connectivity within the SUHI network of urban agglomerations. Methodologically, this research addresses the shortcomings of regional SUHI effects in raster and vector data by introducing a spatial method suitable for the integration and extraction of SUHI patches, and constructs a SUHI interaction network based on the significance and distance of patches. In terms of the theoretical development of regional SUHI effects, the future SUHI patterns are simulated using the Cellular Automata (CA)-Markov model based on current trends. Through analyzing the dynamics of SUHI patch numbers and network development, this study proposes a connectivity-based hypothesis for SUHI development. To verify the effectiveness and applicability of this method, the three major urban agglomerations in China are used as case studies, specifically addressing the following questions:

- 1) Is the process of spatial integration and extraction and the construction of interaction networks suitable for assessing the patterns of SUHI effects? 2) What are the changes, key patches (nodes), and interactions (edges) identified in the SUHI effects in the study area from 2005 to 2020 through this process and methodology? 3) What contributions does this new perspective make to the theoretical development of SUHI effects, and how can it mitigate this excess heat in practice?

2. Methods

2.1. Study area and data

This study focuses on three representative urban agglomerations in China depicted in Fig. 1, namely the Beijing-Tianjin-Hebei (BTH) Region, Yangtze River Delta (YRD), and Guangdong-Hong Kong-Macao Greater Bay Area (GBA), which have experienced rapid urban sprawl and economic development over decades. According to the National Bureau of Statistics of China (<http://www.stats.gov.cn/sj/>), although these three agglomerations encompass merely 12.39% of China's total area, they accounted for 43.99% of the nation's gross regional product in 2020. However, rapid economic development and urbanization have also contributed to prominent and urgent challenges to mitigate the excess heat in urban areas. The three urban agglomerations selected for this study possess diverse climatic backgrounds, natural resource conditions, and development strategies. This makes them ideal research areas for proposing a general hypothesis on SUHI development and provides valuable planning experience for the future development blueprints of other cities. It offers solutions in terms of urban planning, SUHI theory and SUHI governance strategies, ensuring that future urban agglomerations can effectively tackle the SUHI challenges and successfully achieve sustainable development.

The MODIS eight-day composite satellite-based LST product with a spatial resolution of 1 km (version 6, MYD11A2, <https://lpdaac.usgs.gov/products/myd11a2v006/>) in 2005, 2010, 2015 and 2020 was used to analyze the SUHI effects. For this study, the number of available cloud-free images from Aqua and Terra is roughly the same. Considering that the focus of this research is on excess heat, and Aqua's overpass time (1:30 PM) is closer to the daily maximum LST time, we chose to use only the Aqua product in order to ensure the comparability of land surface

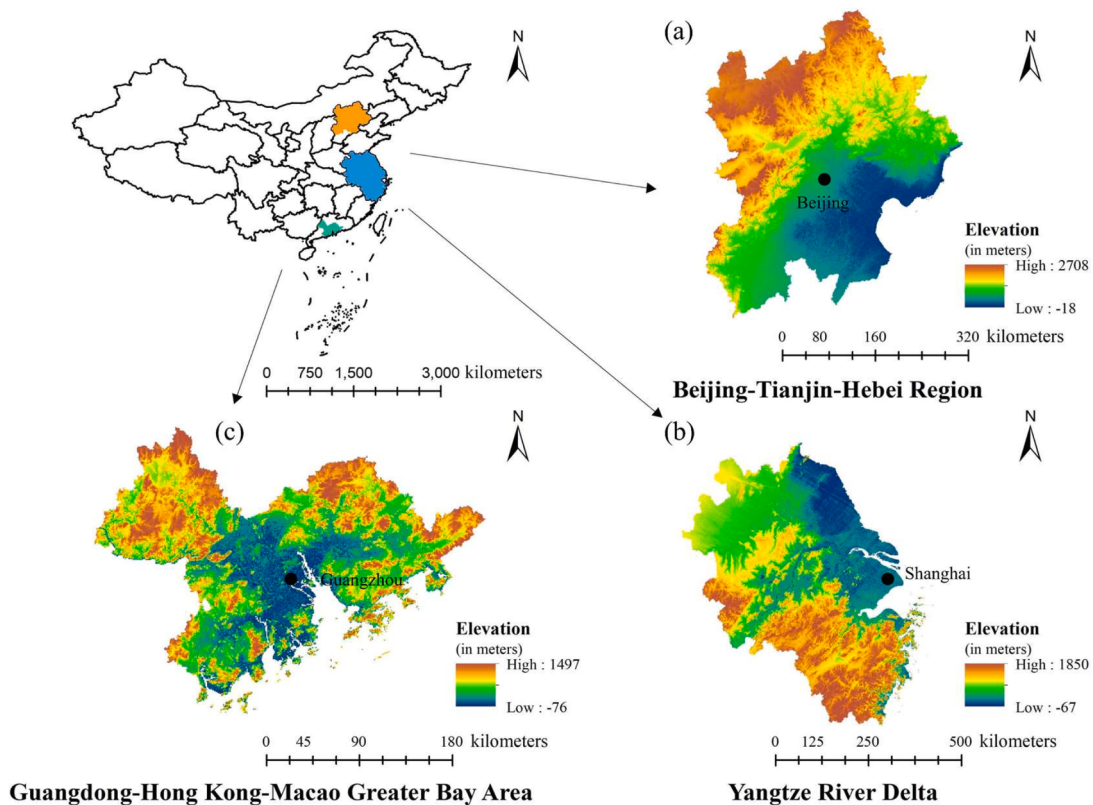


Fig. 1. Geographical locations of the study area: (a) Beijing-Tianjin-Hebei Region; (b) Guangdong-Hong Kong-Macao Greater Bay Area; and (c) Yangtze River Delta.

temperatures across cities in the study area (Zhou et al., 2014; Liu et al., 2024; Peng et al., 2024). The quality of the MODIS LST data has been extensively evaluated by in-situ observations across globe, with a bias generally less than 1 K (Wan, 2014; Yang et al., 2021b). Initially, the MODIS LST data was estimated from images captured in thermal bands 31 and 32 using the generalized split-window algorithm, with the mean retrieval errors within 1.0 K (Wan, 2008). Furthermore, the acquisition of MODIS land surface temperature data is inevitably affected by atmospheric conditions in summer due to abundant rain, leading to missing surface temperature values in some pixels. In each region, we filtered out LST images that were significantly affected by cloud contamination. LST images with more than 30% invalid pixels in each study area were excluded from the research. For each urban agglomeration, the qualifying LST images were used to generate annual LST images using the mean compositing method. The original image dates range from June 26 to September 14 for the years 2005, 2010, and 2015, and from June 25 to September 13 for the year 2020. Then, the comparisons of the SUHI effects were implemented in different regions and periods from both spatial and temporal perspectives, aiming to provide plausible support to verify the hypothesis of cross-scale SUHI evolution in this study. Additionally, the land cover type data at 1 km resolution from 2005 to 2020 with five-year intervals were obtained from the Chinese Academy of Sciences and used as auxiliary data to calculate the SUHII. The LULC dataset is generated through a human-computer interactive visual interpretation method, classifying national land use types into 6 primary categories, 25 secondary categories, and some tertiary categories (see Figure S1). The average classification accuracy for urban, industrial, mining, and residential land use exceeds 85% (<http://www.resdc.cn/DOI>). To be compatible with the SUHI simulation, the original 25 secondary classifications in this dataset were used in the CA-Markov model. The population data in 2020 (with a spatial resolution of 1 km) collected from WorldPop (<https://www.worldpop.org/>) were also used in the simulation of SUHI. The socio-economic statistical data used in this study are sourced from the China City Statistical

Yearbook and the National Bureau of Statistics (<https://data.stats.gov.cn/>). This includes data on the primary, secondary, and tertiary industry Gross Domestic Products (GDPs) and total electricity consumption for the three study areas for the year 2020. All the abovementioned data were integrated spatially and temporally for the analysis.

2.2. Overall methodological framework

The overall methodological framework was divided into two major steps, namely SUHI interactive network construction and SUHI trend prediction (Fig. 2). In the first step, the spatial metrics and average nearest neighbor analysis were successively employed to avoid heavy calculation costs for data compression. Furthermore, based on the compressed data, we synthesized the spatial interaction model and minimum spanning tree (MST) to construct and evaluate the SUHI network. In the second step, we used the Cellular Automata Model to obtain the spatiotemporal dynamics of the SUHI node network.

2.3. Estimation of SUHII using LST data

The intensity of SUHI is typically determined by comparing the temperature differences between urban and rural areas. However, this study faces two primary challenges: firstly, the large study area introduces uncertainty in the delineation of urban-rural boundaries (Liu et al., 2023); secondly, differences in elevation between urban and rural areas can impact the calculation of relative temperature differences (Yao et al., 2018). Consequently, referring to Stewart and Oke (2012), we used the average temperature of green spaces within each urban agglomeration as the region's baseline temperature (Jiang, et al., 2022; Yu et al., 2019). According to the local climate zone SUHII calculation for low-stature vegetation, the green spaces in our study include four categories of surface cover: shrubland, and grasslands with high, medium, and low coverage in our LULC dataset. Moreover, this study has just calculated the SUHII in built-up areas, which include urban land,

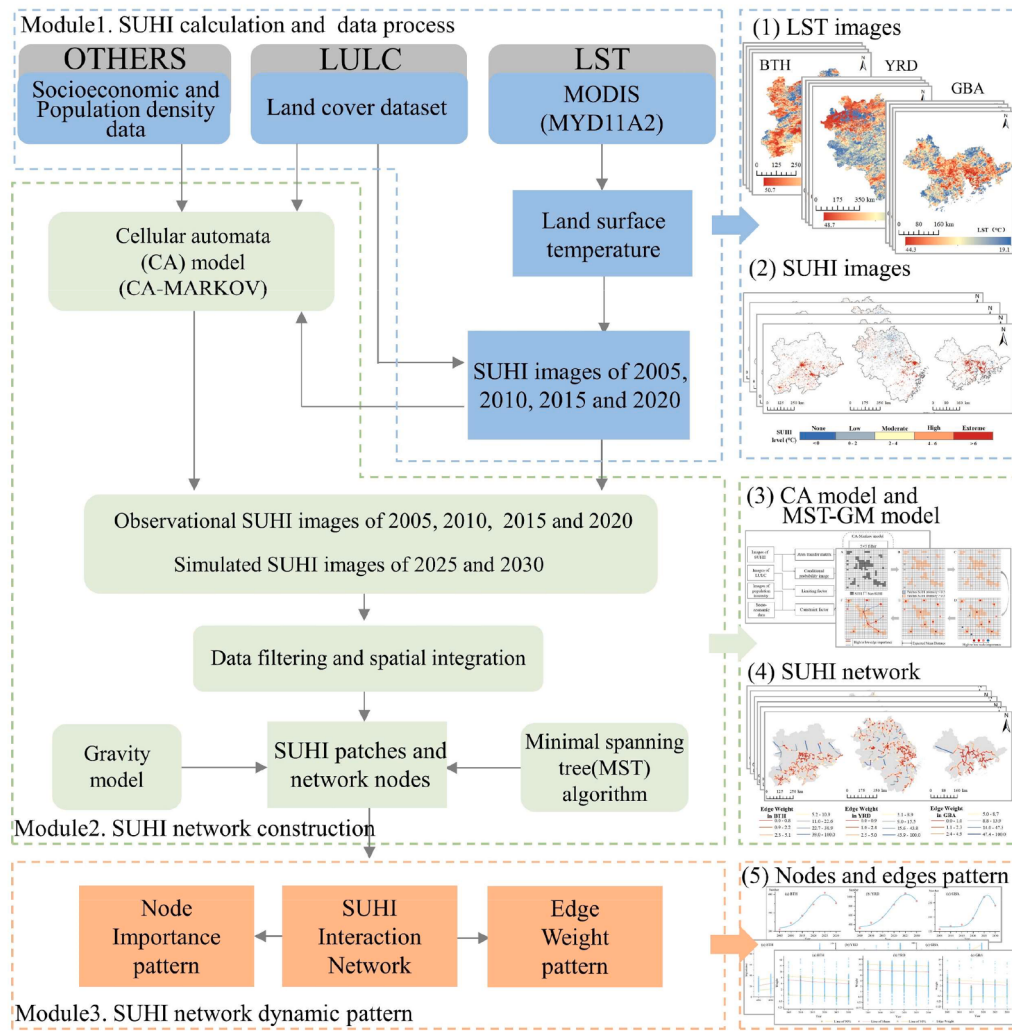


Fig. 2. The methodological framework.

rural settlements, and other constructed areas (such as factories area, large industrial zones, airports, and other special-use lands) as classified in land use and land cover data (see Supplementary materials Figure S1). Therefore, the calculation of SUHII in this study is conducted only within the built-up areas. This decision is made for two main reasons: firstly, excess heat mitigation measures and assessments regarding the connectivity of the SUHI effect can only be applied to artificial surfaces. Secondly, compared to the urban-rural division method and the method of using forest land as the background reference, this approach minimizes the elevation differences within the SUHI regions (see Supplementary materials Figure S2 and Table S1). Consequently, the significant advantage of these measures is the enhancement of the delineation of SUHI effect connectivity and the comparability of SUHII across the three urban agglomerations. The SUHI formula for each pixel is as follows:

$$SUHII_i = T_{bui} - T_{gs} \quad (1)$$

where $SUHII_i$ denotes the SUHII for pixel i in the built-up area, T_{bui} and T_{gs} denote the mean LSTs of the built-up and green space, respectively. And SUHII is divided into five categories displayed in Table 1.

2.4. SUHI interaction network construction

2.4.1. Data filtering and backbone extraction for spatial-integration

The classified SUHI patches generally presented a discrete

Table 1
SUHI classification criterion.

SUHII ($^{\circ}\text{C}$)	SUHI Levels
< 0	No SUHI
0 – 2	Low SUHI
2 – 4	Moderate SUHI
4 – 6	High SUHI
> 6	Extreme SUHI

distribution, including thermal hysteresis and thermal interference, which seriously affected the extraction of SUHI centers. The patch extraction method was inspired by Feng's urban poly-centrality extraction method (Feng et al., 2018). However, the SUHII was not considered during spatial integration in Feng et al. (2018) study, such that there exists an inaccurate identification of the patch importance. We added SUHII as an input for calculating the importance index of SUHI patches, adjusted some parameters based on experiments under the SUHI scenario, and optimized the network generation algorithm. Therefore, we improved this urban poly-centrality extraction method by incorporating SUHII into the process of spatial data filtering and extraction.

For the derived SUHI grid, patches are defined as clusters of contiguous pixels (a-b). Initially, based on the threshold established through our experiment, we eliminate patches with a mean SUHII below 0.5 (b-c). We then compute an importance index for each patch by

factoring in both patch area and SUHII, and subsequently extract the morphological center of each patch (c-d). We iterate through each patch, assessing the hierarchical relationships among patches within each expected mean distance based on their importance index, and perform patch merging accordingly. Finally, we construct an interaction network utilizing the MST-GM approach.

A sensitivity test was conducted to determine the threshold of the SUHI center. We set thresholds at 0-1 degrees Celsius with intervals of 0.1, aiming to reduce computational costs and extract the main SUHII while minimizing information loss. A threshold of 0.5 is closest to the 98% confidence loss (see Figure S3). It is worth noting that in order to extract the SUHI center accurately, patches with an intensity of less than 0.5 will be considered as heat aggregation and removed in this study as shown in Fig. 3 (b-c). According to the Figure S3, we considered the number of pixels and the resulting loss in the SUHI importance index (pixel SUHII multiplied by area) based on different SUHII thresholds.

Subsequently, we calculated the Expected Mean Distance (EMD) for each urban agglomeration at different time periods, thereby defining the spatial scale for data operations. In the nearest neighbor analysis, the optimum shortest average distance d_0 between all patches is defined by Eq. (2) (Mitchell, 2005).

$$d_0 = 0.5 / \sqrt{n/M_0} \quad (2)$$

where n is the total number of patches in an urban agglomeration and M_0 is the minimum enclosed rectangular area containing all patches in an agglomeration. Notably, the calculations of the aforementioned EMD were implemented on each urban agglomerations, to ensure diversity between urban agglomerations and inter-annual variations. Utilizing the above calculated EMD, the essence of this procedure is a spatial systematic sampling of patches by aggregating patches. This approach facilitates the extraction of pivotal patches and nodes in the evolution of the SUHI progression within a specific distance. The resampling and selecting conditions are shown in Eq. (3, 4 and 5)

$$C_i = \prod_{j=1}^n E(I_i - I_j) \text{ s.t. } d_{ij} < d_0 \quad (3)$$

$$E(x) = \begin{cases} 1 & x \geq 0 \\ 0 & x < 0 \end{cases} \quad (4)$$

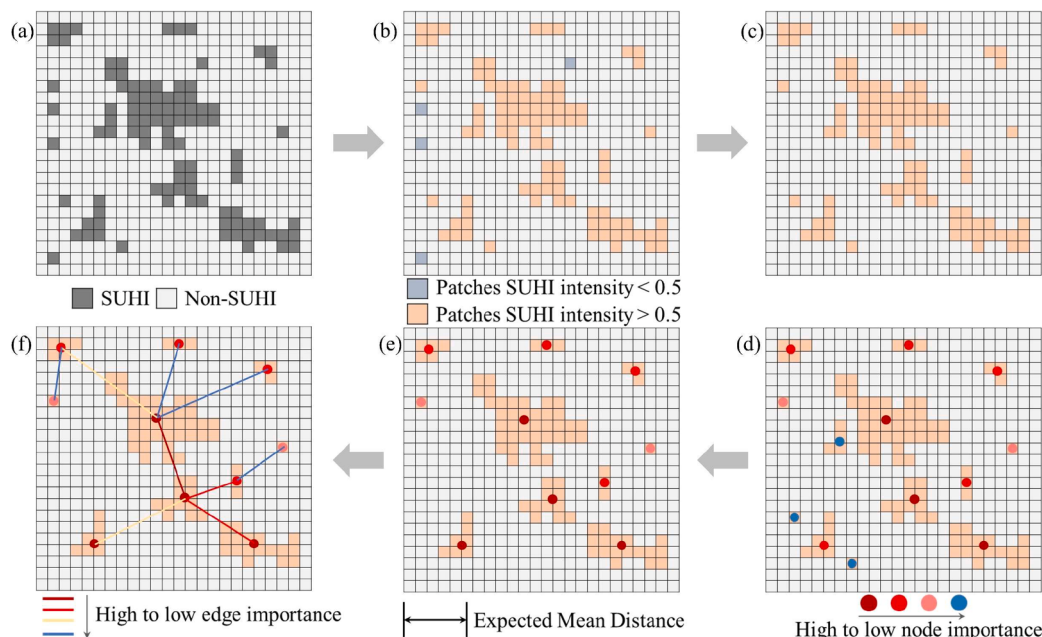


Fig. 3. Illustration of the SUHI network extraction and construction.

$$I_i = M_i \times T_i \quad (5)$$

where I_i and I_j represent the index importance of patch i and j , respectively. n is the total number of patches in an agglomeration, d_{ij} is the distance between patch i and j . d_0 is the expected distance of patches of SUHI in each agglomeration calculated by Eq. (2). The essence of this step is to determine the importance index of all patches at the EMD scale. Patches with low importance within the EMD will be merged into those with high importance, as illustrated in Fig. 3 (c-d).

The patches with a C_i value of 1 will be retained, and the remaining patches will be eliminated, and the retained patches are the ones with the highest importance index within the EMD around them. To ensure consistency, varying EMD was used in different urban agglomerations than fixed thresholds, which possesses a superior advantage in preserving the interannual quantitative correlation of SUHI patches and also enhances the transferability and applicability of the method, even for the regions with different climatic conditions and urban configurations. In addition, in order to compensate for the reduction of the patch area and the loss of intensity caused by the resampling, we supplemented the area of the retained patches and adjusted the intensity by Eq (6 and 7), as shown in the Fig. 3 (d-e).

$$I'_i = I_i + \sum_j I_j \text{ s.t. } 0 < d_{ij} < d_0 \quad (6)$$

$$I'_j = M_j \times T_j \quad (7)$$

where I'_i is the adjusted importance index of the retained patch i . M_j and T_j are the area and intensity of the eliminated patch j , respectively. d_{ij} is the distance between patches i and j . As shown in Figures S4, the number of patches is effectively reduced in all three urban agglomerations after patch extraction, ensuring that the average patch shape index value remains consistent. It indicates the aforementioned data filtering and extraction have extracted the backbone information of SUHI and reduced the computational load effectively, along with the preservation of the data characteristics.

2.4.2. Network construction

After patch extraction, the SUHI network was constructed to explore the SUHI dynamic evolution over the past two decades. Specifically, the

geometric centers of the patches were extracted and deemed as nodes for the SUHI network by connecting the nodes to reflect the interaction strength between SUHI patches. From this basis, we devised an algorithm to the construction of an interaction network among SUHI patches (nodes), by integrating the Minimum Spanning Tree algorithm and the gravity model (MST-GM). The Minimum Spanning Tree (MST) aligns with the basic laws of the gravity model to connect nodes with higher computational efficiency. Moreover, MST error assessment adopts the minimum span rather than the minimum mean square error, which is more suitable for processing actual geographical scenarios. The MST-GM was based on an improved gravity model to quantify the interaction strength between SUHI patches, which is denoted as follows.

$$W_{ij} = \frac{d_{ij}^2}{\sqrt{I_i I_j}} \quad (9)$$

where W_{ij} represents the weight of the edge connecting nodes i and j . d_{ij} is the distance between nodes i and j . I_i and I_j are the importance index of nodes i and j respectively. Through this step, we have transformed data from a grid format into a network composed of nodes and edges, as shown in Fig. 3 (e-f).

In particular, we made some notable modifications compared to the traditional gravity model. First, the reciprocal form was adopted, which facilitates the principal conditions of the MST network construction. Second, the unit dimension that will affect the result is eliminated, and the weight value of the edge is limited to a suitable range by the root operation. Furthermore, by incorporating the intensity and area (importance index) of patches as influencing factors into the model, Tobler's first law of geography has been refined to accommodate the SUHI context.

2.5. SUHI prediction based on CA - Markov model

2.5.1. CA-Markov model

The CA-Markov model is an ensemble model that integrates the Cellular Automata (CA) and Markov chain analysis. The CA model is used to simulate the spatial-temporal process of urban expansion by defining transition rules (Firozjaei et al., 2018). Markov chain analysis is a statistical method used to forecast the probability of various results based on a certain state or set of states in the past (Mushore et al., 2017). By combining these two methods, the CA-Markov model can simulate the spatial distribution of SUHI under different urban development scenarios in various periods.

The future state of a cell is determined upon the current state as well as the states of its neighboring cells. In other words, the prediction of a

cell future state can be perceived by analyzing the correlation between the cell's state and its neighboring relationships. Consequently, the transformation rules of the CA directly influence the results of SUHI prediction. In this study, we calculated the SUHI level transition matrix and the suitability image encompassing influential factors as the transformation rules. The structure of the CA-Markov model utilized is depicted in Fig. 4.

The inputs for the CA-Markov model include four components: the 2020 SUHII raster, the water bodies raster layer (including rivers, lakes, reservoirs, and wetlands) from the LULC, the population density raster layer, and the processed raster layers of primary, secondary, and tertiary GDP and electricity consumption. The numerical data, such as GDP for the primary, secondary, and tertiary industries, along with total electricity consumption, are distributed across 1 km grid, segmented by individual cities. This approach can show the spatial disparities and urban agglomerations between cities, providing a significant socio-economic reference data. This approach shows the developmental disparities between cities and urban agglomerations, providing a significant socio-economic backdrop for understanding regional development differences.

Based on the previously classified five SUHII levels (Table 1), a five-category area transition matrix for SUHI was created. The original SUHII raster data was used as the conditional probability image. Water bodies from the LULC were used as limiting factors, and population density along with socioeconomic data was deemed as constraint factors. Then the values of the influencing factors were normalized to a range of 0–255, and determine the weights between factors using the Analytic Hierarchy Process (AHP). Finally, through weighted linear combination, the heat island conversion probabilities and influencing factor weights for each level can be calculated together with the SUHII maps.

2.5.2. Validation of CA-Markov model

Using year 2015 as the reference year, the distribution of SUHII in 2020 was derived after five iterative calculations, and the result will be compared with the actual conditions in 2020, which can verify the performance of the CA-Markov model, whereas the Kappa index method is also utilized to assess the accuracy of the model. To evaluate the applicability and accuracy of the CA-Markov model, we used 2015 as the base year to iteratively simulate the SUHII in 2020. We compared our results with the actual SUHI observations from 2020, incorporating the Kappa coefficient, Mean Absolute Error (MAE), and Root Mean Square Error (RMSE) to assess the accuracy in both spatial distribution and numerical values, thereby validating the efficacy of our simulation model. The Kappa coefficient shows the consistency of the simulated and

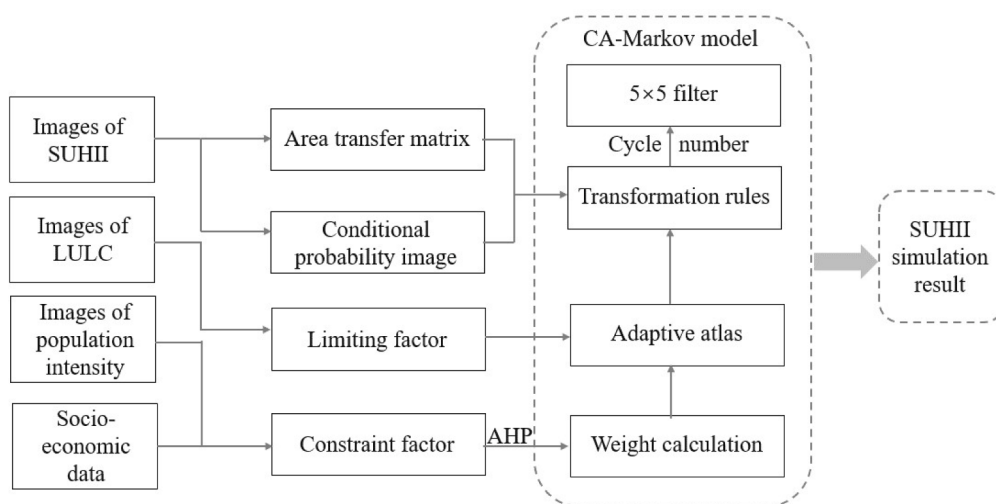


Fig. 4. CA-Markov model technical flow.

observed spatial distribution of SUHI, while MAE and RMSE indicate the numerical error for pixels where spatial consistency is maintained.

3. Results

3.1. Spatiotemporal pattern of SUHI in three urban agglomerations

As Fig. 5 depicted, the spatial patterns of SUHI in these three urban agglomerations present significant increasing trends over the study period. Moreover, the annual average growth rates of SUHI areas in the three regions were 1.01%, 1.41%, and 1.09%, respectively. In areas with dense SUHI patches, the merging of patches into larger SUHI patches

contributes to the area SUHI development. Visually, this phenomenon appears as an expansion from dense areas outward. Notably, new smaller SUHI patches have emerged around the core areas, becoming new growth centers for SUHI areas. By comparing the three urban agglomerations laterally, each region exhibits different spatial heterogeneity, but areas such as coastlines and estuaries tend to show higher SUHI phenomena. The GBA region had the highest annual average proportion of SUHI area, reaching 7.72%, followed by BTH at 6.34%, and YRD at 5.03%.

From a temporal perspective, although the average SUHII increased in all three regions, BTH and GBA experienced the largest increases from 2005 to 2010, reaching 1.79 and 2.36 degrees Celsius, respectively. In

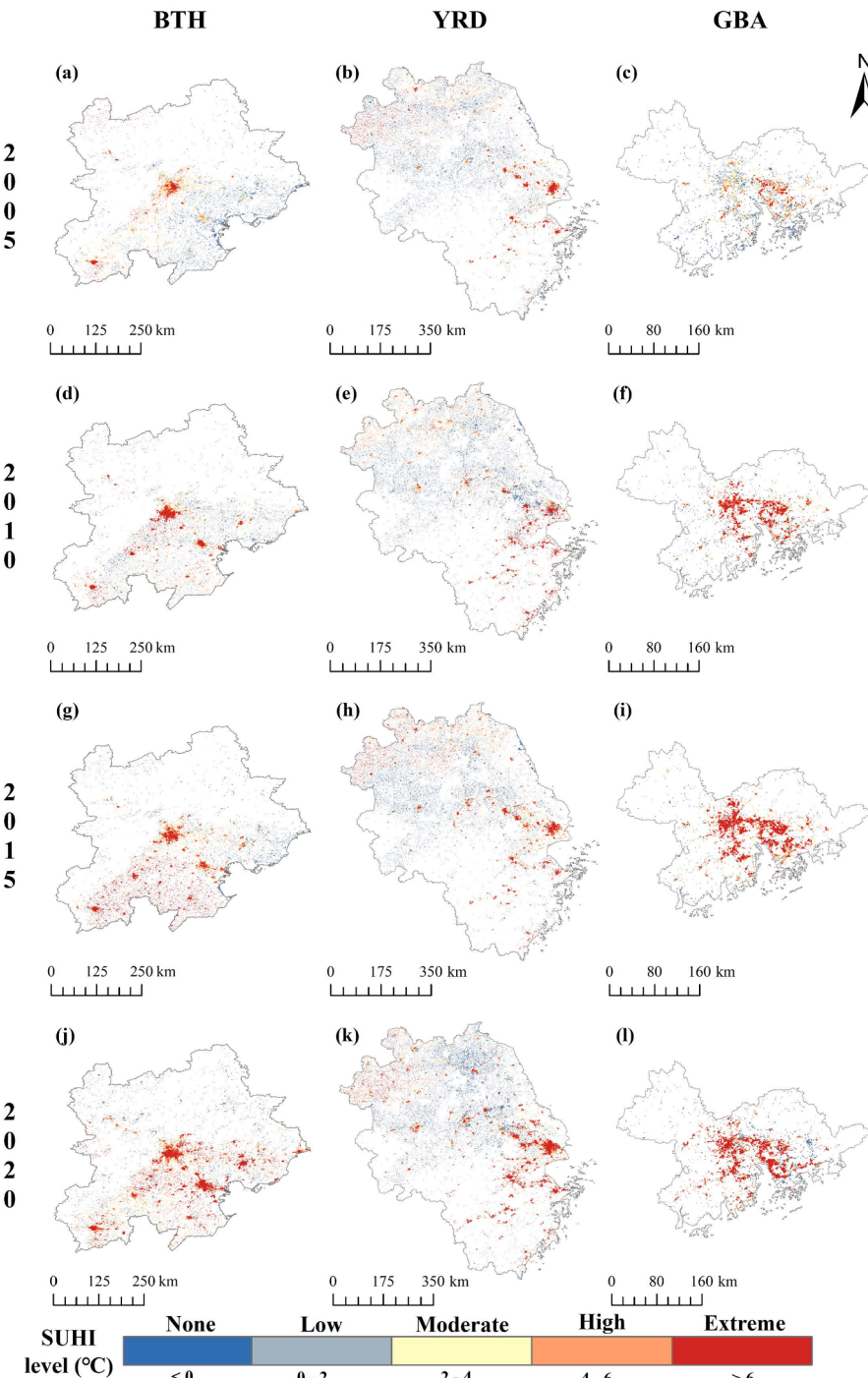


Fig. 5. Spatial evolution of SUHI from 2005 – 2020 in three agglomerations.

contrast, the YRD region has the largest average SUHII increase from 2015 to 2020, reaching 1.56 degrees Celsius. In terms of SUHII levels, in 2005, many areas in the three urban agglomerations were at "moderate" and "high" heat island levels, but by 2010 or later, these areas had upgraded to "extremely high" heat island levels. Newly emerging heat island areas have also experienced similar SUHII level increases over time.

3.2. Spatial interaction network of SUHI

According to our definition of edge weight, the smaller the edge weight, the higher the interaction intensity between the two patches, interpreted as smaller interaction resistance. As shown in Fig. 6, the complexity of the network was increasing manifested by the emergence of new SUHI nodes and the greater interactivity between old nodes. Edges with higher weights are accumulated in high-intensity SUHI

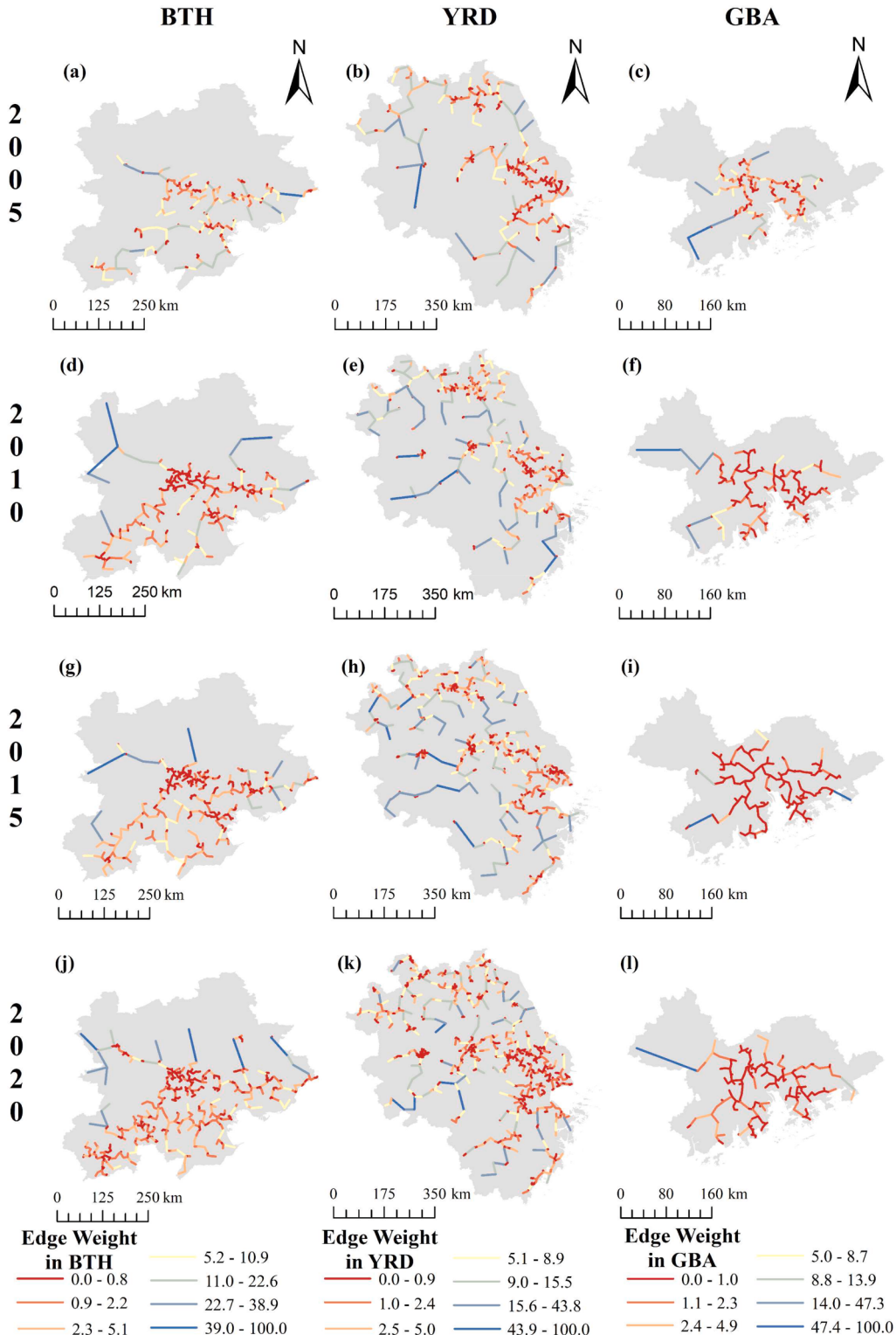


Fig. 6. SUHI interaction network from 2005 – 2020 in three agglomerations.

areas, while new nodes around existing large nodes tend to emerge and dissipate faster. In terms of the evolution pattern of the network, the heat island interaction networks of the three urban agglomerations present similar variations. Around nodes with high weights, the density of nodes and edges is higher. These areas are accompanied by the migration of node positions and structural differentiation. Outside these areas, the main mode of network evolution is the emergence of new nodes and the resulting new connections, which corresponds to the merging and emergence of patches observed in Fig. 5.

Specifically, the SUHI network in the BTH region expanded in the southwest direction with Beijing and Tianjin deemed as accumulation centers from 2005 to 2020. The network exhibits remarkable spatial heterogeneity, which indicates that the heat islands in the southeast region present a more dynamic structure for comparison. Meanwhile, the number of network nodes in BTH reached 494 in 2020, with an average node importance index of 27.1. The edge weight increased by 39.4% compared to 2005. Since 2005, the SUHI network in the YRD has developed a radiating pattern centered around several core cities, including Shanghai, Suzhou, Nanjing and Hefei (see Supplementary materials Figure S6). From 2005 to 2020, the morphology and metrics of this network have undergone significant changes. The average patch importance index increased from 28.7 to 44.5, while the average interaction intensity rose by 14.1%. The network in the GBA region sprawls around the Pearl River Estuary. Compared with the other two urban agglomerations, its interannual network changes are considered smaller, with stronger integrity and stability. Notably, compared with the other two regions, the GBA network has the highest node importance index and the smallest edge weight, with annual averages of 46.9 and 2.2, respectively.

3.3. Simulation of SUHI network dynamics in 2025 and 2030

It is evident that the number of pixels with spatial consistency, the Kappa coefficient, MAE and RMSE remain at a high level, which demonstrates the accuracy of our simulation model in replicating SUHI regions (Table 2). Notably, the model is more accurate in simulating high SUHII values compared to low SUHII values (Fig. 7). However, the overall accuracy is controlled within 5%, which is widely regarded as the threshold for the effectiveness of the CA-Markov model (Rodríguez Eraso et al., 2013; Naboureh et al., 2017; Firozjaei et al., 2018). The MAE and RMSE are lower in the BTH and GBA regions, while the simulation errors in the YRD region are around 2 degrees Celsius. By calculating the average error per pixel divided by the observed SUHI value, we obtained the average errors for these three regions, showing the smallest average error in the BTH region at 1.87%, followed by the GBA region at 2.95%, and the largest in the YRD region at 5.72% (Table 2).

Fig. 8 presents the simulation results and spatial distribution characteristics of the SUHI network in 2025 and 2030. For these three urban agglomerations, the number of nodes in 2025 continues to increase as compared that in 2020, though the growth rate has significantly declined. Additionally, the SUHI accumulation area with higher intensity further expands. This implies that at this stage, the emergence speed of network nodes is more likely to slow down, but the interaction between nodes will become stronger. From 2025 to 2030, the number of nodes in the network tends to decrease, and the interaction between nodes will be further strengthened. This change will profoundly alter the SUHI network structure and development pattern in the core area, with

network structure in this area will tend to be more simplified. In the sub-core area of the cities, the growth of node numbers will slow down, and the edge weights increase. The sub-core area process is exactly what happened in the core area in the previous stage. In the peripheral areas of the network, new nodes appear, leading to changes in the peripheral branches of the network, while the weights between these nodes remain at a stable level.

In the YRD region, the number of SUHI patches increased by 7.9% and 23.6% during 2020-2025 and 2010-2015, respectively. However, the corresponding areas increased by 30.2% and 19.7% respectively. This difference indicates that patches in the core area will be merged, combining as the larger patches, despite that the number and area of heat island patches cannot be used as the sole indicators for evaluating heat islands. Furthermore, in our simulation, Shanghai, Hangzhou, and Suzhou formed a strongly connected network, and with the increase in edge weights, the number of nodes in this area continued to decrease. In addition, similar phenomenon appears in Beijing, Langfang, Guangzhou, and Shenzhen cities (see Figure S6). These areas have the growth potential to develop into a large SUHI node in the future or may reach a stable state.

Since the area or number of heat island patches cannot adequately describe the development status of individual SUHI patch, we adopted the node importance index defined during network generation to measure the numerical changes of heat islands. As shown in Fig. 9 (a-c), after data normalization, the importance index of SUHI node in the three regions shows an upward trend with an exponential growth based on the mean fitting curve - a SUHI node importance as the product of patch area and intensity. This indicates that the area and intensity of heat islands in the study area have been continuously strengthened. We selected a 90% confidence interval to determine the degree of distribution aggregation. Specifically, the distribution of node importance index values in the BTH region is more dispersed. The YRD region maintains a relatively stable level of dispersion. The GBA region shows a more concentrated distribution of importance index over the study period. The SUHI interaction network is composed of nodes in heat island patches and edges represented as the interaction intensity between heat islands. Due to the reciprocal calculation mode used, the weight of the edge reflects the interaction resistance between two heat island patches. The smaller the weights, the stronger the interaction between heat islands.

Fig. 9 (d-f) illustrates the distribution patterns of edge weights within the network. By applying the same nonlinear stretching to the vertical axis, we can observe comparable distribution patterns across three regions, all of which exhibit a declining trend in edge weights. Additionally, the confidence intervals for BTH and GBA have narrowed, indicating a more concentrated distribution in these regions compared to YRD, where the confidence interval boundaries remain stable. Moreover, there are the differences in the lower boundary values of the three regions. This was because a fixed threshold was not chosen when we spatially integrated the heat islands; instead, the EMD was used as the spatial integration scale. Therefore, the lower boundary of the confidence interval can be considered as the threshold for the merging of SUHI. The merging threshold of SUHI in the YRD is considered as the largest, followed by the BTH, with the GBA being the smallest. Projecting the three curves into the linear coordinate system, the lower boundary of the confidence interval remains at a stable level, while the upper boundary continues to shrink downwards, narrowing the gap of the confidence interval.

Through the changes in the number of SUHI patches or network

Table 2
CA-Markov model simulation accuracy.

Agglomerations	Number of observed pixels	Number of simulated pixels	Number of consistent pixels	Kappa	MAE	RMSE	Average error
BTH	30801	32443	26216	0.86	0.99	1.20	1.87%
YRD	58590	54265	50247	0.86	2.11	2.32	5.72%
GBA	9804	11694	9017	0.92	1.17	1.31	2.95%

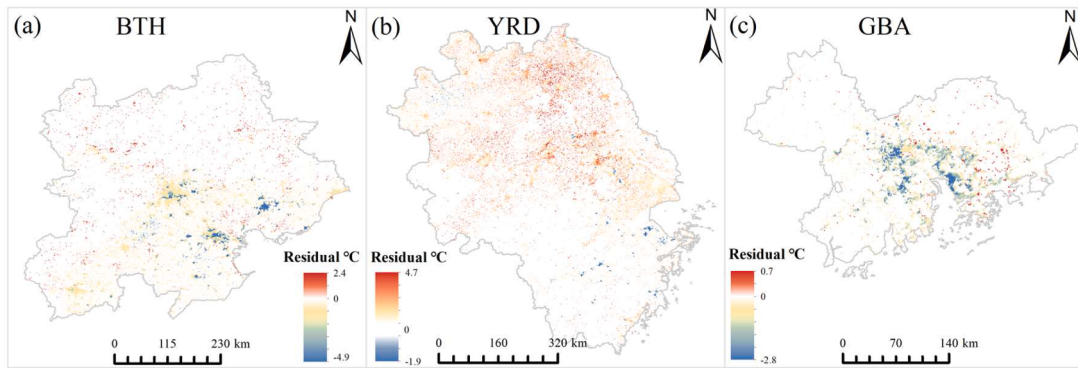


Fig. 7. Simulation residuals from the comparison of the simulated and observed SUHI values in 2020.

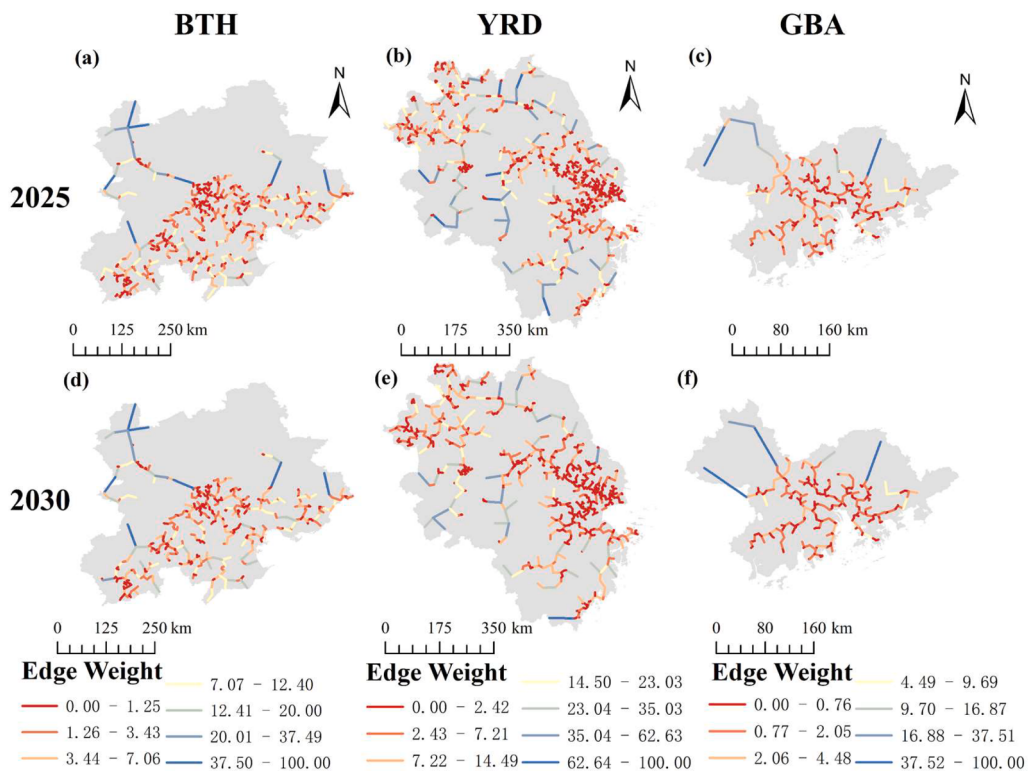


Fig. 8. Simulated interaction SUHI network from 2025 – 2030 in three agglomerations.

nodes, we can roughly observe the evolution of the SUHI networks in the three regions, as shown in Fig. 9 (g-i). The results indicate that the Gaussian curve fits well into the changes in the number of nodes in all scenarios. Under the prediction model we constructed, an expected decreasing number of patches and nodes in the three urban agglomerations in the future is forecasted. Furthermore, the node importance index and edge weight show a strengthening trend, providing supportive evidence for the merging of SUHI. The evolution patterns of SUHI node numbers are also different among the three regions. In the GBA region, the number of nodes remained at a low level from 2005 to 2015, and experienced rapid growth from 2015 to 2025. The evolution patterns of the number of network nodes in the BTH and YRD regions seem to be similar, but there are significant differences in the number of nodes and the magnitude of changes in the three regions. The GBA region has the least number of nodes, followed by the BTH region, and the YRD region has the most nodes. It is worth noting that the number of nodes only reflects the complexity of the SUHI network, while a smaller number of nodes does not imply a smaller SUHI area and intensity.

4. Discussion

4.1. From grid expansion to network growth

It has generally recognized that most current studies on the SUHI effect are based on a patch perspective using raster and vector analyses (Chen, Sun, & Lu, 2019; Saura & Pascual-Hortal, 2007). For example, these studies quantify the shape index and size of urban blue-green space patches to mitigate the SUHI effect, and achieve optimal local cooling through the best combination and configuration of blue-green spaces. However, understanding these excess heat mitigations first requires identifying or locating the most critical SUHI patches, and then making anthropogenic changes to the surface types to alleviate the SUHI effect.

In this study, we proposed a non-threshold spatial integration method for SUHI extraction using expected average distance, and incorporated the area and intensity of SUHI patches to calculate the importance of individual heat island nodes. By combining the improved gravity model and the minimum spanning tree algorithm, we

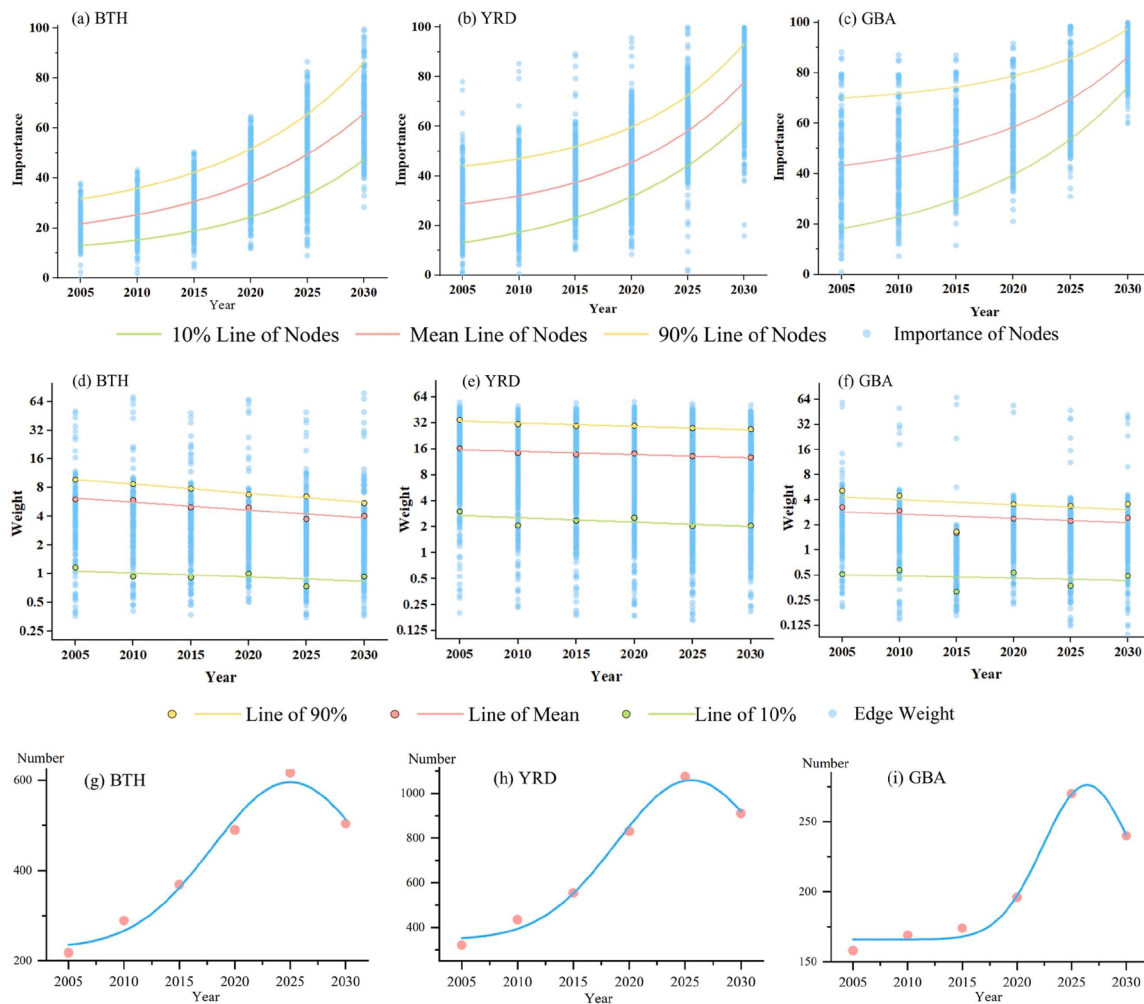


Fig. 9. The numerical distribution of nodes' relative importance in SUHI network (a-c). The numerical distribution of edge weight in SUHI network (d-f). Node number of SUHI network (g-i).

constructed the SUHI network in three urban agglomerations. The evolution of network nodes and edges could reveal the dynamics of development patterns and trends of SUHI in the study area. Unlike the previous studies, we focused on the extraction and identification of individual SUHI patches (nodes). By integrating the geographical spaces, the dynamics of the SUHI network was established based on the potential laws of individual SUHI development and interaction between SUHI.

Although an intensification of the SUHI effect at different spatial scales (Wang, 2021), SUHI assessment solely based on intensity evidently does overlook the geographical characteristics of SUHI. There is a surging need for decision-makers to further monitor the changing trends, spatial features to formulate sustainable management strategies of SUHI under the rapid urbanization. New theories and detection methods should be proposed to provide a basis for future urban agglomeration planning, with regard of the spatiotemporal dynamic analysis of SUHI indices.

The dynamic development process of SUHI is evaluated by extracting the main network of SUHI. This approach has the following significant merits. Firstly, our method introduces intensity and morphological features to assist network construction, enabling the generation of SUHI networks based on geographical scenarios. Secondly, the method uses an adaptive computational scale, namely the minimum expected distance, allowing the scale threshold of spatial integration to be determined by the data itself. The three urban agglomerations have different SUHI index patterns so the expected average distance for each period supports

data compression and aggregation, ensuring the optimal extraction scale for each urban agglomeration. Thirdly, the development pattern of the continuum, through data normalization, makes interannual comparability meaningful. For example, according to our research results, the three regions present similar distribution patterns from 2020 to 2025 in Fig. 6, 7. In summary, the algorithm proposed in this paper promotes the development of SUHI dynamic monitoring in urban agglomerations and is an important technical support for improving SUHI development theory.

4.2. Implications of urban development strategies for SUHI networks

Based on the impact of urban development policies and strategies, our method draws credible conclusions, fully explaining the “unimodal” phenomenon (Fig. 9 g-i). In the three urban agglomerations, the spatial distribution characteristics and expansion trends of SUHI are easily observed intuitively (Figs. 7 and 8). However, quantifying the dynamic process of SUHI patch expansion and fusion has always been a barrier to solve the theory of SUHI development. By constructing a SUHI interaction network in urban agglomerations, the fusion and interaction patterns between patches can be revealed. The sub-core area of the urban agglomeration is the most active area for SUHI development, and the number of patches and interaction intensity profoundly affect the structure of the SUHI network. This indicates that an increase in the area and intensity of heat island patches would also increase the network's dependence on specific patches within the urban agglomeration, and the

merging process reduces the number of patches, indirectly affecting the heat island network structure. In addition, this study also simulated the development of SUHI in 2025 and 2030. The active area of the SUHI extends from the core area, and the development of the SUHI has a significant delay as compared with urbanization. In addition, the confidence intervals in the three regions show different patterns (Fig. 9 a-c), which correspond to the different development patterns and strategy formulations of three urban agglomerations. BTH has gradually transitioned from a development pattern centered on Beijing to a multi-core development pattern centered on Tianjin and Shijiazhuang. This leads to a multi-polar pattern of heat island growth. At the same time, these three growth poles maintain a considerable geographical distance, so the probability of SUHI patches merging between the three cities is considered very low. Thus, new nodes will not be able to be swallowed by old large nodes. This method of breaking away from the old growth pole and developing a new growth pole brings out a new phenomenon of SUHI node importance diffusion. For the GBA (Fig. 9 c), the node importance value of GBA in 2005 is the highest among the three research areas. With the development of urbanization, new growth poles mostly appear surrounding old nodes. Due to the close geographical distance and strengthened interaction, these new growth poles are more inclined to the merges of old nodes. The disappearance of small nodes leads to the rise of the lower boundary of confidence interval, whereas the large nodes per se together with the merge of surrounding small nodes have the potential rise of the upper boundary of the confidence interval. For YRD region, the pattern showed that the merging of old large nodes such as Shanghai leads to the rise of the upper boundary of the confidence interval. Due to the change in the development strategy of the urban agglomeration, the emergence of new growth poles is speculated to appear at the places such as Wuhan, the northern part of Suzhou, and Jiangxi, generating a synchronous rise of the lower boundary of the confidence interval.

The pattern changes of SUHI have been extensively studied, with land cover and land use changes being highly correlated. Impervious surfaces and blue-green spaces have consistently been core factors in explaining the spatiotemporal changes of SUHI (Deilami et al., 2018). On one hand, urban development strategies lead to changes in urban substrates and surface characteristics. On the other hand, urban policies also alter population distribution, resulting in increased energy consumption that exacerbates the SUHI effect (Yang et al., 2021a). Therefore, SUHI network changes are influenced by the combined effects of urban environmental and socio-economic factors, which is why it is essential to consider the socio-economic context of cities when using the CA-Markov model for simulations. It remains uncertain whether the flow of population and materials between cities will enhance interactions between SUHI patches. However, it is certain that, due to the stronger association of population distribution with socio-economic factors, mitigating the SUHI effect cannot rely solely on improving the urban surface environment. Public resources such as healthcare facilities and education are equally important (Liu et al., 2024).

4.3. SUHI growth hypothesis with urban development

The SUHI network is composed of nodes representing heat island patches and edges denoting the merging resistance between nodes. Correspondingly, we divide the development of the SUHI network into two “behaviors”. One is the appearance of new nodes, and the other is the integrations between nodes. The patterns shown in the three regions mentioned above actually depend on which of these two “behaviors” predominant. For the BTH region, the speed of new node appearance is greater than the speed of node merging. Furthermore, as shown in Fig. 9 (d), the BTH region has higher edge weights and greater interaction resistance between nodes, which also aligns to our hypothesis. In the GBA region, node merging dominants, which can also be seen from the smaller edge weights. Notably, the differences brought about by these two “behaviors” can support the development strategies and policy

support of the urban agglomerations, providing recommendation to the development of satellite cities and regional multi-polar growth policies. Natural geographical conditions, such as mountain barriers and geographical distance, will reduce the possibility of merging.

Based on the above discussion, we propose an ideal hypothesis for SUHI development to demonstrate the macroscopic impact of the two “behaviors” of “emerge” and “merge” on the quantity of the heat island network. SUHI patches emerged in the first stage of urban development due to the changes in the underlying surface (Rizvi et al., 2020; Yu et al., 2019). Due to the abundance of urban development space and the distance between patches, the rate of patches emergence increases further until reaching the highest speed of patch emergence in Stage i, while the emergence is still the major pattern of SUHI development. Subsequently, in Stage ii (Fig. 10), due to the smaller urban space and the smaller distance between patches caused by the expansion of patches, the merge speed of patches is accelerated. The number of SUHI patches reached the maximum when the speed of patch emergence and merging are equal. With the further development of urban space and the improvement of surface utilization rate, the emergence of new patches slows down and the merging of original patches speeds up. Patch merging predominates in Stage iii, which suggests that the dominant pattern of SUHI development is merging, and shortly accompanied by a rapid decline in patch numbers. There is a “unimodal” phenomenon in this process, while the change in the number of nodes can be fitted into a Gaussian curve. Our research results show that the evolution of SUHI has a certain regularity.

In conjunction with the urban development process, small patches of heat accumulation emerged in the initial state due to the underlying surface changes based on urbanization and anthropogenic heat emissions, which formed the foundation of the current SUHI structure. Higher surface utilization and anthropogenic heat emission intensity lead to some of the heat accumulation becoming the third-level of SUHI. Due to the urbanization process, the existing SUHI patches with sufficient distance are further upgraded. Subsequently, new SUHI patches emerge and the total number of SUHI patches increases rapidly. Due to the limited distance, SUHI patches start to integrate slowly in the next stage. As the fused larger patch has more opportunities to become closer to other small ones and growth focuses on the intensity of patches, the speed of coalescence increases quickly, along with the emergence of new SUHI patches slows down. Thus, the number of SUHI patches is expected to reach a maximum after this stage and is likely to generate a rapid decline in the near future. Owing to the gradual slowdown in urban growth or counter urbanization (Fielding, 1982), the coalescence speed slows down, and in turn it will take a long time for SUHI patches to aggregate into one single center covering the whole region.

The dynamic development process of SUHI provides new

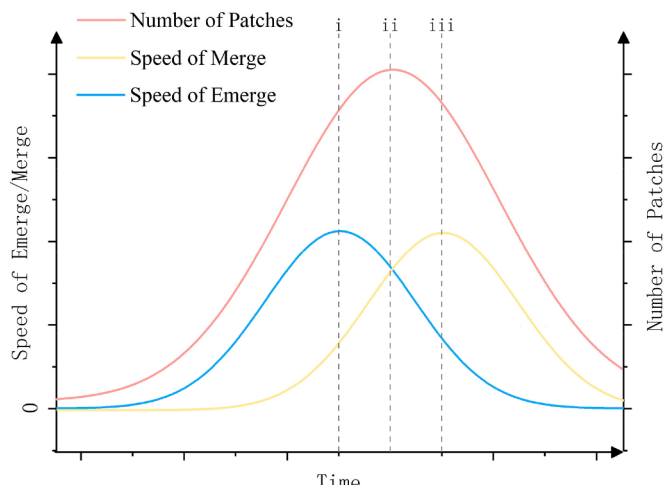


Fig. 10. Schematic diagram of SUHI unimodal ideal hypothesis.

perspectives and greater capabilities for urban agglomeration in SUHI governance. Previous SUHI governance focused too much on the shape and intensity of individual patches, and the potential of key patches was inevitably underestimated. This study takes large SUHI patches as nodes to provide a possible SUHI spread scenario in urban agglomerations. In order to achieve sustainable urban thermal environment management, recommendations are put forward from the following aspects. First, through the governance of important patches, the development of the SUHI network can be fundamentally controlled in a more effective way which aims to reduce regional SUHI patch merging and ensure a moderate SUHII level. Additionally, evacuating urban core areas is also beneficial for sustainable urban thermal environment management which is also highly suggested (You & Yang, 2017). Specific measures can be considered for implementation, like distributing urban functions, reducing the land use intensity of the core area, and slowing down the consolidation of SUHI patches in the core area, as well as establishing satellite cities (Su et al., 2017). It is important to note that the planning of satellite cities may mitigate the excess heat in core areas. However, due to factors such as low intensity, small size, and the considerable distance from surrounding SUHI patches, these areas may not necessarily become identifiable hotspots within the network or merge with core areas to form larger patches within a certain timeframe. Lastly, establishing a cross-administrative governance body can maintain SUHI governance measures implemented across the region. In terms of the application of the method, This study proposes an adaptive computational scale-space integration that exhibits strong scalability to accommodate different data scales and urban agglomerations. In terms of the extended applications in other regions, due to the spatial integration based on adaptive computation scales, this method could be catered for scalability and adaptability to different urban agglomerations. In addition, urban policymakers and planners can adopt and use the developed method to simulate future SUHI based on current trends, thus mitigating the urban SUHI effect by disrupting key patches and the connectivity within the urban SUHI network.

4.4. Limitations and future studies

Considering the universality of the research results and the general hypothesis on SUHI network growth, we chose MODIS LST data to meet the research requirements. It should be noted that data resolution significantly affects the identification of SUHI patches, the delineation of built-up areas, and the calculation of background temperatures. Therefore, data with finer spatio-temporal resolution are supposed to be involved to provide more implications for the dynamic evolution of SUHI.

Methodologically, although calculating SUHII only within built-up areas reduces the impact of elevation to some extent, it is difficult to totally eliminate the possibility of some built-up areas being at different altitudes, which could lead to deviations in SUHII values. Furthermore, the improved gravity model used to measure interactions between patches does not account for the effects of actual geographical features, such as rivers, lakes, and mountains, which can influence or hinder interactions, or merging of SUHI patches and reduce model accuracy. These could be spatial factors that constrain the SUHI effect. Future research could develop an obstruction network model of SUHI effects using natural elements like blue-green spaces to compare model accuracy. Additionally, this study attempts to simulate future SUHI patterns based on current trends. However, to achieve accurate predictions, there is a lack of consideration for certain meteorological and environmental factors, such as precipitation and soil texture, as well as the interactions between these environmental factors and their contribution in SHII.

5. Conclusion

This study attempts to identify and analyze key SUHI patches through network construction and to explore the development patterns

of SUHI by examining changes in network nodes and edges. First, data integration was utilized to extract SUHI patches, which can also reduce the computational load of the network. Then, an interaction network of SUHI patches was constructed using the MST-GM method. Finally, the CA-Markov model was employed to simulate the SUHI network for the years 2025 and 2030 under current trends. The conclusions are summarized as follows. Firstly, the dynamic patterns of the SUHI network in the three urban agglomerations have significant spatial heterogeneity. The speed of new node appearance in the BTH region is greater than the merging speed, the node merging speed in the GBA region is larger than the appearance speed, while the appearance and merging speeds of nodes in the YRD region are at similar rates. Additionally, due to natural geography and urban policies, the heat island merging thresholds varied among those three urban agglomerations, with the GBA region being the smallest, followed by BTH and YRD. Finally, the appearance and merging of nodes are key indicators that determine the dynamic pattern of SUHI, and they affect the SUHI network morphologically and structurally. Implementing cooling measures in sub core areas of the city, through approaches such as blue-green space planning or the decentralization of urban functions, is the most effective and efficient way to mitigate SUHI effect which will also significantly reduce the merging of SUHI patches.

Compared to other studies, the theoretical significance of the method proposed in this research lies in the shift from a patch-based perspective to a network-based perspective, rather than relying on the patch perspective based on raster or vector data. In practical terms, identifying key nodes of the SUHI effect is a prerequisite for implementing urban heat mitigation measures. This approach allows for effective integration with urban climate adaptation planning, particularly when urban areas continue to expand and urban agglomerations emerge. The method proposed in this paper offers a new perspective for understanding the development patterns of SUHI, and it can be widely adopted to research and practice in other regions.

CRediT authorship contribution statement

Kang Zou: Writing – review & editing, Writing – original draft, Visualization, Validation, Methodology, Formal analysis, Data curation, Conceptualization. **Xinyu Yu:** Writing – review & editing, Methodology, Formal analysis, Conceptualization. **Man Sing Wong:** Writing – review & editing, Writing – original draft, Validation, Supervision, Methodology, Funding acquisition, Formal analysis, Conceptualization. **Kai Qin:** Writing – review & editing, Methodology, Formal analysis. **Rui Zhu:** Writing – review & editing, Methodology, Conceptualization. **Songyang Li:** Writing – review & editing, Conceptualization.

Declaration of competing interest

The authors declare that they have no known competing financial interests or personal relationships that could have appeared to influence the work reported in this paper.

Acknowledgments

We sincerely thank NASA for providing the MODIS LST data and the Resource and Environmental Science Data Platform for the LULC data. The data sources are also given in this paper. This study is supported by the General Research Fund (Grant No. 15603920 and 15609421), and the Collaborative Research Fund (Grant No. C5062-21GF) from the Research Grants Council, Hong Kong, China; and the funding support from the Research Institute for Sustainable Urban Development, The Hong Kong Polytechnic University, Hong Kong, China (Grant No. 1-CD81).

Supplementary materials

Supplementary material associated with this article can be found, in the online version, at doi:10.1016/j.scs.2024.105926.

Data availability

Data will be made available on request.

References

- Bartesaghi-Koc, C., Osmond, P., & Peters, A. (2020). Quantifying the seasonal cooling capacity of 'green infrastructure types'(GITS): An approach to assess and mitigate surface SUHI in Sydney, Australia. *Landscape and urban planning*, 203, Article 103893.
- Cao, X., Onishi, A., Chen, J., & Imura, H. (2010). Quantifying the cool island intensity of urban parks using ASTER and IKONOS data. *Landscape and urban planning*, 96(4), 224–231.
- Chen, L., Sun, R., & Lu, Y. (2019). A conceptual model for a process-oriented landscape pattern analysis. *Science China Earth Sciences*, 62, 2050–2057.
- Cornes, I. C., & Cook, B. (2018). Localising climate change: heatwave responses in urban households. *Disaster prevention and management: An international journal*, 27(2), 159–174.
- Debbage, N., & Shepherd, J. M. (2015). The SUHI effect and city contiguity. *Computers, Environment and Urban Systems*, 54, 181–194.
- Deilami, K., Kamruzzaman, M., & Liu, Y. (2018). SUHI effect: A systematic review of spatio-temporal factors, data, methods, and mitigation measures. *International journal of applied earth observation and geoinformation*, 67, 30–42.
- Dewan, A., Kiselev, G., Botje, D., Mahmud, G. I., Bhuiyan, M. H., & Hassan, Q. K. (2021). Surface SUHII in five major cities of Bangladesh: Patterns, drivers and trends. *Sustainable Cities and Society*, 71, Article 102926.
- Fan, Y., Li, Y., Bejan, A., Wang, Y., & Yang, X. (2017). Horizontal extent of the urban heat dome flow. *Scientific reports*, 7(1), 11681.
- Fang, C., Zhou, C., Gu, C., Chen, L., & Li, S. (2017). A proposal for the theoretical analysis of the interactive coupled effects between urbanization and the eco-environment in mega-urban agglomerations. *Journal of Geographical Sciences*, 27, 1431–1449.
- Feng, Y., Wu, S., Wu, P., Su, S., Weng, M., & Bian, M. (2018). Spatiotemporal characterization of megaregional poly-centrality: Evidence for new urban hypotheses and implications for polycentric policies. *Land Use Policy*, 77, 712–731.
- Fielding, A. J. (1982). Counterurbanisation in western Europe. *Prog. plann.*, 17, 1–52.
- Firozjaei, M. K., Kiavarz, M., Alavipanah, S. K., Lakes, T., & Qureshi, S. (2018). Monitoring and forecasting heat island intensity through multi-temporal image analysis and cellular automata-Markov chain modelling: A case of Babol city, Iran. *Ecological indicators*, 91, 155–170.
- Hu, J., Yang, Y., Zhou, Y., Zhang, T., Ma, Z., & Meng, X. (2022). Spatial patterns and temporal variations of footprint and intensity of surface SUHI in 141 China cities. *Sustainable Cities and Society*, 77, Article 103585.
- Imhoff, M. L., Zhang, P., Wolfe, R. E., & Bounoua, L. (2010). Remote sensing of the SUHI effect across biomes in the continental USA. *Remote sensing of environment*, 114(3), 504–513.
- Jiang, L., Xie, M., Chen, B., Su, W., Zhao, X., & Wu, R. (2024). Key areas and measures to mitigate heat exposure risk in highly urbanized city: A case study of Beijing, China. *Urban Climate*, 53, Article 101748.
- Jiang, S., Zhan, W., Dong, P., Wang, C., Li, J., Miao, S., ... Wang, C. (2022). Surface air temperature differences of intra-and inter-local climate zones across diverse timescales and climates. *Building and Environment*, 222, Article 109396.
- Lai, J., Zhan, W., Voogt, J., Quan, J., Huang, F., Zhou, J., ... Lee, X. (2021). Meteorological controls on daily variations of nighttime surface SUHI. *Remote Sensing of Environment*, 253, Article 112198.
- Li, L., Zha, Y., Zhang, J., Li, Y., & Lyu, H. (2020). Using prophet forecasting model to characterize the temporal variations of historical and future surface SUHI in China. *Journal of Geophysical Research: Atmospheres*, 125(23), Article e2019JD031968.
- Li, T., Chen, C., & Cai, W. (2022). The global need for smart heat-health warning systems. *The Lancet*, 400(10362), 1511–1512.
- Li, B., Zhang, B., Yin, L., & Chang, J. (2023). Assessing heat risk for residents of complex urban areas from an accessibility-based perspective. *Sustainable Cities and Society*, 88, Article 104278.
- Lin, Y., Jim, C. Y., Deng, J., & Wang, Z. (2018). Urbanization effect on spatiotemporal thermal patterns and changes in Hangzhou (China). *Building and Environment*, 145, 166–176.
- Liu, H., He, B. J., Gao, S., Zhan, Q., & Yang, C. (2023). Influence of non-urban reference delineation on trend estimate of surface SUHI: A comparison of seven methods. *Remote Sensing of Environment*, 296, Article 113735.
- Liu, H., Huang, B., Zhan, Q., Gao, S., Li, R., & Fan, Z. (2021). The influence of urban form on surface SUHI and its planning implications: Evidence from 1288 urban clusters in China. *Sustainable cities and society*, 71, Article 102987.
- Liu, Q., Xie, M., Peng, J., Zhou, X., Yang, K., Zhu, R., & Liu, Y. (2024). Revealing the urban heat exposure risk network: Exploring the possibility of mitigate heat-related risks form a network perspective. *Sustainable Cities and Society*, Article 105592.
- Mazdiyasni, O., & AghaKouchak, A. (2015). Substantial increase in concurrent droughts and heatwaves in the United States. *Proceedings of the National Academy of Sciences*, 112(37), 11484–11489.
- Meng, Q., Zhang, L., Sun, Z., Meng, F., Wang, L., & Sun, Y. (2018). Characterizing spatial and temporal trends of surface SUHI effect in an urban main built-up area: A 12-year case study in Beijing, China. *Remote Sensing of Environment*, 204, 826–837.
- Mitchell, A. (2005). The Esri guide to GIS analysis, Volume 2: Spatial measurements and statistics (second).
- Montgomery, M. R. (2008). The urban transformation of the developing world. *science*, 319(5864), 761–764.
- Mushore, T. D., Odindi, J., Dube, T., & Mutanga, O. (2017). Prediction of future urban surface temperatures using medium resolution satellite data in Harare metropolitan city, Zimbabwe. *Building and Environment*, 122, 397–410.
- Naboureh, A., Rezaei Moghaddam, M. H., Feizizadeh, B., & Blaschke, T. (2017). An integrated object-based image analysis and CA-Markov model approach for modeling land use/land cover trends in the Sarab plain. *Arabian Journal of Geosciences*, 10, 1–16.
- Oke, T. R., Mills, G., Christen, A., & Voogt, J. A. (2017). *Urban climates*. Cambridge university press.
- Peng, J., Cheng, X., Hu, Y., & Corcoran, J. (2022). A landscape connectivity approach to mitigating the SUHI effect. *Landscape Ecology*, 37(6), 1707–1719.
- Peng, J., Qiao, R., Wang, Q., Yu, S., Dong, J., & Yang, Z. (2024). Diversified evolutionary patterns of surface SUHI in new expansion areas of 31 Chinese cities. *npj Urban Sustainability*, 4(1), 14.
- Quan, J., Chen, Y., Zhan, W., Wang, J., Voogt, J., & Wang, M. (2014). Multi-temporal trajectory of the SUHI centroid in Beijing, China based on a Gaussian volume model. *Remote Sensing of Environment*, 149, 33–46.
- Rizvi, S. H., Fatima, H., Iqbal, M. J., & Alam, K. (2020). The effect of urbanization on the intensification of SUHI: Analysis by LULC on Karachi. *Journal of Atmospheric and Solar-Terrestrial Physics*, 207, Article 105374.
- Rodríguez Eraso, N., Armenteras-Pascual, D., & Alumbreros, J. R. (2013). Land use and land cover change in the Colombian Andes: dynamics and future scenarios. *Journal of Land Use Science*, 8(2), 154–174.
- Saura, S., & Pascual-Hortal, L. (2007). A new habitat availability index to integrate connectivity in landscape conservation planning: comparison with existing indices and application to a case study. *Landscape and urban planning*, 83(2–3), 91–103.
- Shen, Y. (2024). Separation of the Urbanization Effects on Thermal Environment. *Sustainable Cities and Society*, Article 105585.
- Stewart, I. D., & Oke, T. R. (2012). Local climate zones for urban temperature studies. *Bulletin of the American Meteorological Society*, 93(12), 1879–1900.
- Streutker, D. R. (2003). Satellite-measured growth of the SUHI of Houston, Texas. *Remote sensing of Environment*, 85(3), 282–289.
- Su, S., Liu, Z., Xu, Y., Li, J., Pi, J., & Weng, M. (2017). China's megaregion policy: Performance evaluation framework, empirical findings and implications for spatial polycentric governance. *Land Use Policy*, 63, 1–19.
- Sun, R., Xie, W., & Chen, L. (2018). A landscape connectivity model to quantify contributions of heat sources and sinks in urban regions. *Landscape and urban planning*, 178, 43–50.
- Sun, Z., Zhang, X., Li, Z., Liang, Y., An, X., Zhao, Y., ... Li, D. (2024). Heat exposure assessment based on high-resolution spatio-temporal data of population dynamics and temperature variations. *Journal of Environmental Management*, 349, Article 119576.
- Wan, Z. (2008). New refinements and validation of the MODIS land-surface temperature/emissivity products. *Remote sensing of Environment*, 112(1), 59–74.
- Wan, Z. (2014). New refinements and validation of the collection-6 MODIS land-surface temperature/emissivity product. *Remote sensing of Environment*, 140, 36–45.
- Wang, K., Li, Y., Luo, Z., Yin, S., & Chan, P. W. (2018a). Harmonic analysis of 130-year hourly air temperature in Hong Kong: detecting urban warming from the perspective of annual and daily cycles. *Climate Dynamics*, 51, 613–625.
- Wang, Y., Du, H., Xu, Y., Lu, D., Wang, X., & Guo, Z. (2018b). Temporal and spatial variation relationship and influence factors on surface SUHI and ozone pollution in the Yangtze River Delta, China. *Science of the Total Environment*, 631, 921–933.
- Wang, Z. H. (2021). Compound environmental impact of urban mitigation strategies: Co-benefits, trade-offs, and unintended consequence. *Sustainable Cities and Society*, 75, Article 103284.
- Yang, J., Wang, Y., Xue, B., Li, Y., Xiao, X., Xia, J. C., & He, B. (2021a). Contribution of urban ventilation to the thermal environment and urban energy demand: Different climate background perspectives. *Science of The Total Environment*, 795, Article 148791.
- Yang, J., Hu, L., & Wang, C. (2019). Population dynamics modify urban residents' exposure to extreme temperatures across the United States. *Science Advances*, 5(12), eaay3452.
- Yang, Q., Huang, X., & Tang, Q. (2019). The footprint of SUHI effect in 302 Chinese cities: Temporal trends and associated factors. *Science of The Total Environment*, 655, 652–662.
- Yang, Q., Huang, X., Yang, J., & Liu, Y. (2021b). The relationship between land surface temperature and artificial impervious surface fraction in 682 global cities: spatiotemporal variations and drivers. *Environmental Research Letters*, 16(2), Article 024032.
- Yao, R., Wang, L., Huang, X., Niu, Y., Chen, Y., & Niu, Z. (2018). The influence of different data and method on estimating the surface SUHII. *Ecological Indicators*, 89, 45–55.
- Yao, R., Wang, L., Huang, X., Niu, Z., Liu, F., & Wang, Q. (2017). Temporal trends of surface SUHI and associated determinants in major Chinese cities. *Science of the Total Environment*, 609, 742–754.
- You, H., & Yang, X. (2017). Urban expansion in 30 megacities of China: Categorizing the driving force profiles to inform the urbanization policy. *Land Use Policy*, 68, 531–551.

- Yu, Z., Yao, Y., Yang, G., Wang, X., & Vejre, H. (2019). Spatiotemporal patterns and characteristics of remotely sensed region heat islands during the rapid urbanization (1995–2015) of Southern China. *Science of the Total Environment*, 674, 242–254.
- Yu, Z., Zhang, J., Yang, G., & Schlaberg, J. (2021). Reverse thinking: a new method from the graph perspective for evaluating and mitigating regional surface heat islands. *Remote Sensing*, 13(6), 1127.
- Yue, W., Liu, X., Zhou, Y., & Liu, Y. (2019). Impacts of urban configuration on SUHI: An empirical study in China mega-cities. *Science of the Total Environment*, 671, 1036–1046.
- Zhou, D., Bonafoni, S., Zhang, L., & Wang, R. (2018). Remote sensing of the SUHI effect in a highly populated urban agglomeration area in East China. *Science of the Total Environment*, 628, 415–429.
- Zhou, D., Xiao, J., Frolking, S., Zhang, L., & Zhou, G. (2022). Urbanization contributes little to global warming but substantially intensifies local and regional land surface warming. *Earth's Future*, 10(5), Article e2021EF002401.
- Zhu, S., Yang, Y., Yan, Y., Causone, F., Jin, X., Zhou, X., & Shi, X. (2022). An evidence-based framework for designing urban green infrastructure morphology to reduce urban building energy use in a hot-humid climate. *Building and Environment*, 219, Article 109181.
- Zinzi, M., Agnoli, S., Burattini, C., & Mattoni, B. (2020). On the thermal response of buildings under the synergic effect of heat waves and SUHI. *Solar Energy*, 211, 1270–1282.
- Zhou, D., Zhao, S., Liu, S., Zhang, L., & Zhu, C. (2014). Surface urban heat island in China's 32 major cities: Spatial patterns and drivers. *Remote Sensing of Environment*, 152, 51–61.